

# The Three-Dimensional Morphometry and Cell–Cell Communication of the Osteocyte Network in Chick and Mouse Embryonic Calvaria

Yasuyo Sugawara · Ryoko Ando · Hiroshi Kamioka · Yoshihito Ishihara ·  
Tadashi Honjo · Noriaki Kawanabe · Hiroshi Kurosaka · Teruko Takano-Yamamoto ·  
Takashi Yamashiro

Received: 11 March 2010 / Accepted: 25 January 2011 / Published online: 22 February 2011  
© Springer Science+Business Media, LLC 2011

**Abstract** The study of osteocytes has progressed in chicks. We examined whether chick osteocyte data can be applied to other species. We used mice for comparison because they are common clinical tools in biomedical research and useful for future study. We analyzed the three-dimensional (3D) osteocyte network and gap junctional intercellular communication (GJIC) in living embryonic calvaria for the anatomical features. Embryonic parietal bones were stained with fluorescently labeled phalloidin and observed using confocal laser scanning microscopy. GJIC between osteocytes in chick and mouse parietal bone was assessed using fluorescence recovery after photobleaching (FRAP). The values for one chick and mouse osteocyte, respectively, were calculated as follows: cell processes  $1,131 \pm 139 \mu\text{m}$ ,  $2,668 \pm 596 \mu\text{m}$ ; surface area  $1,128 \pm 358 \mu\text{m}^2$ ,  $2,654 \pm 659 \mu\text{m}^2$ ; and cell volume  $455 \pm 90 \mu\text{m}^3$ ,  $1,328 \pm 210 \mu\text{m}^3$ . The density of 3D osteocyte processes in the bone matrix was not significantly different. FRAP analysis showed dye coupling among osteocytes in chick and mouse bone. The fluorescence intensity recovered to  $49.0 \pm 2.4\%$  in chicks and

$39.9 \pm 2.4\%$  in mice after 5 minutes. Fluorescence recovery was similar within 4 minutes. The difference in osteocyte size between the two species might have affected their functions. Osteocyte processes in the two species may sense similarly changes in the exterior environment. We successfully conducted morphological and functional analyses of the osteocyte network in chicks and mice. The size of the osteocytes in bone differed between the two species.

**Keywords** Osteocyte · Osteoblast · Bone architecture/structure

Osteocytes are the most abundant cells in bone and are involved in multiple functions, including calcium sensing, regulation of osteoid matrix maturation and mineralization, and mechanosensing [1–5]. Chicks have been widely used as experimental models for the examination of the roles of osteocytes in vivo and in vitro, at least in part. This is because chick osteocytes are characteristically detected by a specific antibody, OB7.3, in a strain-specific manner, which facilitates the isolation of primary osteocytes using the panning method [6]. This method was modified to isolate chick osteocytes by serial digestion of calvariae [7]. Such isolation facilitated investigations of their cytoskeleton, cell–cell communication between osteocytes, and response to mechanical stimuli [8, 9]. Chick calvariae are also useful for observing the three-dimensional (3D) distribution of osteocytes in bone tissue because they are thin ( $50\text{--}60 \mu\text{m}$ ) and flat. These anatomical characteristics provided advantages in observing their structures using confocal laser scanning (CLS) microscopy from the surface to deeper layers [10, 11]. Furthermore, live imaging of fluorescent labels is also available and dye transfer

---

The authors have stated that they have no conflict of interest.

---

Y. Sugawara (✉) · R. Ando · H. Kamioka · Y. Ishihara ·  
T. Honjo · N. Kawanabe · H. Kurosaka · T. Yamashiro  
Department of Orthodontics and Dentofacial Orthopedics,  
Okayama University Graduate School of Medicine, Dentistry,  
and Pharmaceutical Sciences, 2-5-1 Shikata, Okayama-City,  
Okayama 700-8525, Japan  
e-mail: yasuyo\_s@md.okayama-u.ac.jp

T. Takano-Yamamoto  
Division of Orthodontics and Dentofacial Orthopedics, Tohoku  
University Graduate School of Dentistry, 4-1 Seiryomachi,  
Aoba-ku, Sendai-City, Miyagi 980-8574, Japan

mediated by connexin 43 has also been observed in living cells of the calvariae [12].

On the other hand, mice are a laboratory animal species that is closely related to humans, and genetically engineered mice are critical and popular tools for biomedical research that genotypically mimic human physiology and/or disease. Morphological differences in osteocyte processes have been reported in dentin matrix protein-1 knockout mice with increased fibroblast growth factor-23 expression in osteocytes [13]. Such findings have thus contributed to a better understanding of the physiology of osteocytes and/or the osteocyte network. Hence, mice are definitely the most potent laboratory tool. Meanwhile, chicks still have some advantages, especially in bone research, because use of embryonic chicks easily allows certain experimental manipulations of developing skeletal tissues. The embryonic head is oriented outward in the hatching egg, and the calvariae can be easily accessed after removal of the overlying eggshell. Such easy accessibility of the target tissues allows the experimental manipulation of developing calvariae, such as gene transfection and drug application, which increases the value of chick calvariae as an experimental model. It is valuable, therefore, to understand the species-specific differences in the morphology and functions of osteocytes.

Previous reports have compared osteocyte morphology and distribution among various species [14–20]. Most of these reports have observed osteocyte morphology and distribution using two-dimensional (2D) data [14–18]. Some reports studying 3D osteocyte morphology and distribution calculated their value from 2D data without unified age [19, 20]. Thus, it remains unclear whether the 3D osteocyte network in bone varies according to species and whether results from chick osteocytes can be applied to osteocytes from other species. We compared the osteocyte network in bone between chicks and mice, which were thought to be well suited to the experiments. The 3D morphology of osteocytes in bone has not been reported in mice. In addition, understanding osteocyte networks and their gap junctional intercellular communication (GJIC) may be important for determining the biological properties of bone. Consequently, we compared not only the 3D structures of the osteocyte networks present in bone but also their functions and we compared our results between chicks and mice.

## Materials and Methods

### Skeletal Preparation

E14-day-old to P0-day-old chicks (white leghorn) and E15-day-old to P0-day-old mice (C57BL/6J) were processed

for skeletal examination by double staining with alizarin red S (Nacalai Tesque, Kyoto, Japan) and alcian blue 8GX (Sigma, St. Louis, MO), as follows. Embryos were fixed in 95% ethanol overnight. Cartilage was then stained with 0.015% alcian blue 8GX in glacial acetic acid:95% ethanol (1:4) for 1–2 days, then washed in 95% ethanol for 3 hours. Soft tissues were macerated in 2% potassium hydroxide (KOH) until the bones became visible. Calcified bone was stained with 0.005% alizarin red S in 1% KOH overnight. Any excess stain was removed by immersion in 1% KOH for 3–7 days, and then the specimen was stored in 20% glycerin in 1% KOH.

### Histological Examination

Parietal bone samples were obtained from E14- and E16-day-old chicks and E15- and E17-day-old mice and washed with alpha-modified minimum essential medium ( $\alpha$ -MEM; Invitrogen, Carlsbad, CA) to remove nonadherent cells. Then, segments of bone were fixed in 4% paraformaldehyde and processed with methyl methacrylate (MMA) for histological analysis. MMA-embedded calvariae were sliced using the RM2255 microtome (Leic Microsystems, Richmond Hill, Canada). After the samples had been sliced at a thickness of 6  $\mu$ m, Villanueva-Goldner staining was performed, and the stained sections were observed under a DP70 and BX60 microscopy system (Olympus, Tokyo, Japan).

### Preparation of Bone Fragments for Morphometric Analysis

Calvariae were obtained from 16-day-old embryonic chicks or 17-day-old embryonic mice and washed with  $\alpha$ -MEM to remove nonadherent cells. Calvariae used for morphometric analysis were obtained from 11 chicks and 12 mice. After stripping off the periosteum, the parietal bone was obtained from the calvariae and trimmed into 3  $\times$  3-mm pieces in chick and 2  $\times$  2-mm pieces in mouse for further use.

### Fluorescence Staining and CLS Images

Chick and mouse calvarial fragments were fixed with 3% paraformaldehyde in PBS overnight and then permeabilized by incubation in 0.5% Triton X-100 in phosphate-buffered saline (PBS) for 10 minutes. Fragments were rinsed and stained for 2 days at 4°C with a 1:100 dilution of Texas red-X-conjugated phalloidin (excitation wavelength 595 nm, emission wavelength 615 nm; Molecular Probes, Eugene, OR) in PBS containing 1% BSA. After rinsing with PBS, samples were embedded in fluorescence mounting medium (Dako, Carpinteria, CA) containing

1 mg/mL p-phenylenediamine dihydrochloride (Sigma) and then viewed immediately.

Confocal optical sectioning was performed with a Fluoview FV500 CLS microscopy system (Olympus) equipped for differential interference contrast (DIC) microscopy with a PlanApo objective (60 $\times$ , N.A. = 1.4). The refraction index of the immersion medium (Olympus) was 1.516. Theoretical resolutions for the  $x$ - and  $y$ -axes and for the  $z$ -axis were 0.414 and 0.400  $\mu\text{m}$ , respectively. The frame size of the image was 146.2  $\times$  146.2  $\mu\text{m}$  with an eight-bit color depth. Confocal images were taken with a 0.3- $\mu\text{m}$  step size and processed four times with Kalman averaging. Confocal optical sectioning was performed from the bone side of the osteoblast surface into the bone compartment. Images were digitally processed using Adobe Photoshop CS2 software (Adobe Systems, Mountain View, CA).

### 3D Reconstruction and Morphometric Analysis of the Osteocyte Network

The 3D structure of the osteocyte network was reconstructed from CLS images using IMARIS software (Bitplane, Zurich, Switzerland), as reported previously [11]. The number of processes that radiate from one osteocyte was counted by rotating the 3D-reconstructed fluorescent model. One osteocyte was analyzed per calvaria for the chicks ( $n = 6$ ) and the mice ( $n = 7$ ). In addition, the volume of the bone compartment occupied by one osteocyte was calculated by dividing the volume of the bone compartment by the number of osteocytes in it. Taking one region per animal, 10 regions and 12 regions, each containing several osteocytes, were analyzed for chicks ( $n = 10$ ) and mice ( $n = 12$ ), respectively. IMARIS allows recognition of the center of mass in each osteocyte. Therefore, the point-to-point distances between osteocytes were calculated. The cell-to-cell distances were analyzed in 32 different regions in chicks ( $n = 11$ ) and mice ( $n = 12$ ).

Neuron Tracer (Bitplane) software was used to measure the length of osteocyte processes, as reported previously [11]. We employed this software to obtain a dendritic model of the osteocyte network by mapping fluorescence-positive sites. From the dendritic model, Neuron Tracer automatically measured the total length of the osteocyte processes. We selected regions that contained several osteocytes for our analysis of osteocyte process length in both chicks ( $n = 11$ ) and mice ( $n = 10$ ). To calculate the length of osteocyte processes, we divided the total length of the osteocyte processes by the volume of the analyzed bone compartment. It is difficult to determine where one osteocyte process ends and another begins. Therefore, the length of osteocyte processes was reported as the length per 1  $\mu\text{m}^3$  of bone compartment.

In addition, Surpass (Bitplane) software was used to quantify the surface area and volume of osteocytes including osteocyte processes, as reported previously [11]. We analyzed regions containing several osteocytes from chicks and mice ( $n = 10$  each). It was necessary to perform volume and surface area corrections because of elongation of the  $x$ -,  $y$ -, and  $z$ -axes for the Surpass data. We calculated approximate volume and surface area correction values using the method described in our previous report [11]. In brief, the volume and surface area of the osteocyte cell body were calculated using correction values obtained from 2.0- $\mu\text{m}$  fluorescent beads. Then, the volume and surface area of the osteocyte cell processes were calculated using correction values obtained from 0.5- $\mu\text{m}$  fluorescent beads. The volume corrections for 0.5- and 2.0- $\mu\text{m}$  beads were 0.30 and 0.41, respectively. The surface area corrections for 0.5- and 2.0- $\mu\text{m}$  beads were 0.54 and 0.62, respectively. The cell body volume correction was 0.41, and the cell process volume correction was 0.30. The cell body surface area correction was 0.62, and the cell process surface area correction was 0.54. We then morphometrically analyzed the osteocytes using the obtained correction values. We analyzed the surface areas and volumes of osteocytes in bone compartment units of 1  $\mu\text{m}^3$ .

### Calculation of Morphometric Data for a Single Osteocyte

The average total length of the processes, average surface area, and average volume per osteocyte were thus determined by calculating the bone compartment volume occupied by one osteocyte, multiplying the length of processes, the surface area, and volume per unit volume of bone.

### FRAP Analysis of Osteocytes in Parietal Bone

Quantitative fluorescence recovery after photobleaching (FRAP) analysis [21] was used to assess GJIC between osteocytes in parietal bone, as previously described [12]. Calvariae used for FRAP analysis were obtained from chicks and mice ( $n = 10$  and 15, respectively). Parietal bones were loaded with 5.0  $\mu\text{M}$  of calcein acetoxymethyl ester (calcein-AM, Molecular Probes) for 15 minutes at room temperature, then washed in  $\alpha$ -MEM to remove the excess dye. Bone fragments were subsequently incubated for 45 minutes in  $\alpha$ -MEM with 2% fetal bovine serum (FBS) at 37°C. After loading of calcein-AM into osteocytes in parietal bone, fluorescently labeled osteocytes were visualized. In each experiment, fluorescence recovery was assessed at 1-minute intervals.

The recovery of fluorescence within a bleached osteocyte was calculated using the following equation:

$$\% \text{ Recovery} = [(F_t - F_0)/(F_i - F_0)] \times 100 (\%)$$

% Recovery was defined as the fraction of molecules that were replaced during the time course of the experiment,  $F_t$  was the normalized fluorescence intensity after photobleaching,  $F_0$  was the theoretical fluorescence intensity immediately following bleaching, and  $F_i$  was the initial fluorescence intensity before photobleaching. All calculated rates were corrected for the loss of fluorescence by unbleached control osteocytes, and the recovery curves of the fluorescent intensity were expressed as the average percentage (mean  $\pm$  SE) recovery rate of the treated cells.

### Statistical Analysis

The Mann–Whitney  $U$ -test was used to compare the results of the morphologic and FRAP analyses. Asterisks indicate a significant difference compared with osteocytes in chick parietal bone ( $P < 0.05$ ). Significance tests were performed using statistical analysis software (StatView; SPSS, Inc., Chicago, IL).

## Results

### Observation of the Mineralization Process in Chick and Mouse Skulls

Chick and mouse embryo skulls were stained with alizarin red S and alcian blue 8GX (Fig. 1). Figure 1a–c shows chick embryos and newborns, and Fig. 1d–f shows mouse embryos and newborns. The arrowhead indicates the parietal bone. Chick parietal bone was still not mineralized at E14 (Fig. 1a) but was almost mineralized at E16 (Fig. 1b). Meanwhile, mouse parietal bone was still not mineralized at E15. The mineralization process of mouse parietal bone

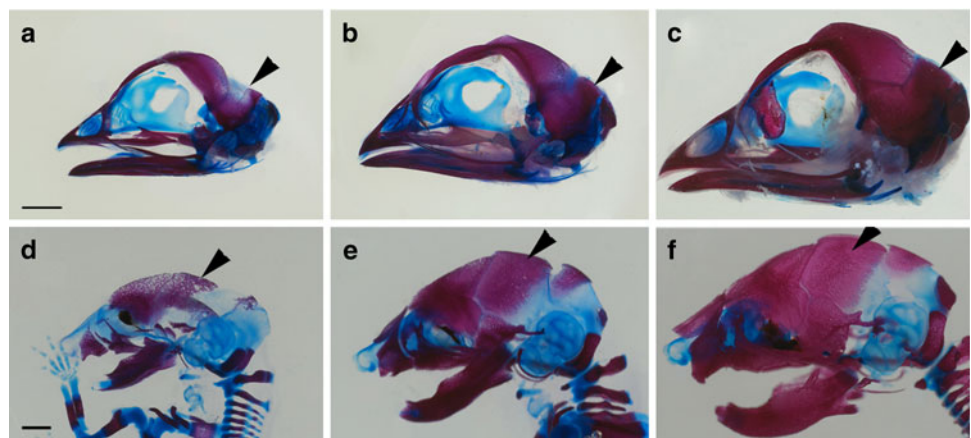
was almost complete by E17 and parietal bone formation at E17 was similar to that at P0 (Fig. 1e, f).

Figure 2 shows Villanueva–Goldner-stained sections. Figure 2a, b shows chick parietal bone sections, and Fig. 2c, d shows mouse parietal bone sections. Most of the bone was composed of osteoid in the E14 chick and E15 mouse parietal bone sections (red area in Fig. 2a, c). Figure 2b, d (E16 chick and E17 mouse, respectively) shows a significant reduction in osteoid area over bone area and increased mineralization (green area). Therefore, chick parietal bone at E16 and mouse parietal bone at E17 were used to observe the osteocyte network (Figs. 1b, e, 2b, d).

### Observation of 3D Osteocyte Network in Chick and Mouse Embryo Parietal Bones Using IMARIS

Bone cells in chick and mouse parietal bone were fluorescently labeled with phalloidin. Figure 3 shows IMARIS images of osteocytes in chick and mouse parietal bone reconstructed from image volumes collected from the osteoblast layer to a 9- $\mu\text{m}$  depth using CLS microscopy. Figure 3a shows the 3D osteocyte network in chick parietal bone, and Fig. 3b shows the 3D osteocyte network in mouse parietal bone. The 3D osteocyte shape appears as suborbicular cells with numerous processes in Fig. 3a, b. The distance between the osteocytes in the chick parietal bone was smaller than that in mouse parietal bone. The mean cell-to-cell distance from one cell to the adjacent cells was  $23.5 \pm 6.1 \mu\text{m}$  in chicks and  $39.6 \pm 11.6 \mu\text{m}$  in mice ( $n = 32$  and  $32$ , respectively) (Table 1). The distance in chick osteocytes was significantly shorter than that in mouse osteocytes ( $P < 0.05$ ). The average number of processes radiating from a single osteocyte was  $52.7 \pm 6.4$  in the chick and  $49.7 \pm 9.7$  in the mouse ( $n = 6$  and  $7$ , respectively) (Table 1). This number was not significantly different between the chick and mouse. In addition, a single osteocyte occupied  $4,691 \pm 935 \mu\text{m}^3$  in the chick ( $n = 10$ ) and

**Fig. 1** Mineralization process of chick (a–c) and mouse (d–f) skulls. a–c Images show bone stained with alizarin red and alcian blue. Chick skull at E14 (a), E16 (b), and P0 (c). d–f Mouse skull at E15 (d), E17 (e), and P0 (f). Arrowheads show the parietal bones. Bar in a = 5 mm, d = 1 mm



**Fig. 2** Villanueva-Goldner-stained histological sections of embryonic parietal bone. Chick parietal bone sections at E14 (**a**) and E16 (**b**). Mouse parietal bone sections at E15 (**c**) and E17 (**d**). Red area is the osteoid area, green area is the mature mineralized area. Bar in **a** = 100  $\mu\text{m}$

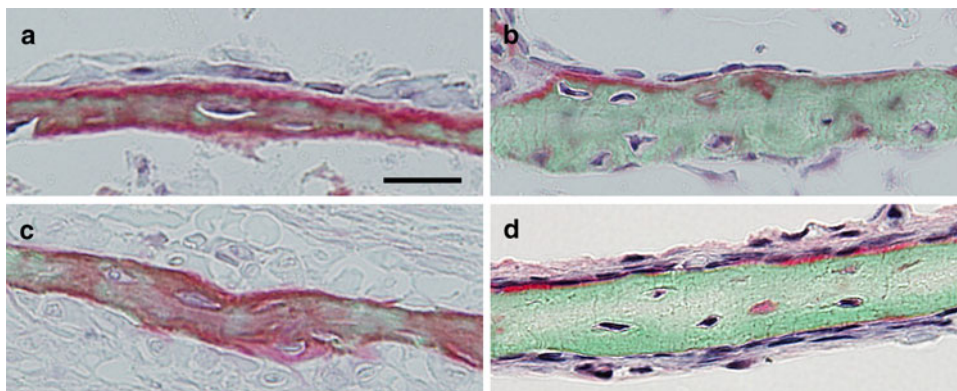


**Fig. 3** 3D reconstruction of the osteocyte network using IMARIS software. CLS images from osteoblast layers up to 9  $\mu\text{m}$  in depth were used for reconstruction. Fluorescent images show cells stained with Texas red-X phalloidin. **a** 3D reconstruction of an osteocyte network in chick parietal bone at E16. **b** 3D reconstruction of an osteocyte network in mouse parietal bone at E17. Bar in **a** = 20  $\mu\text{m}$

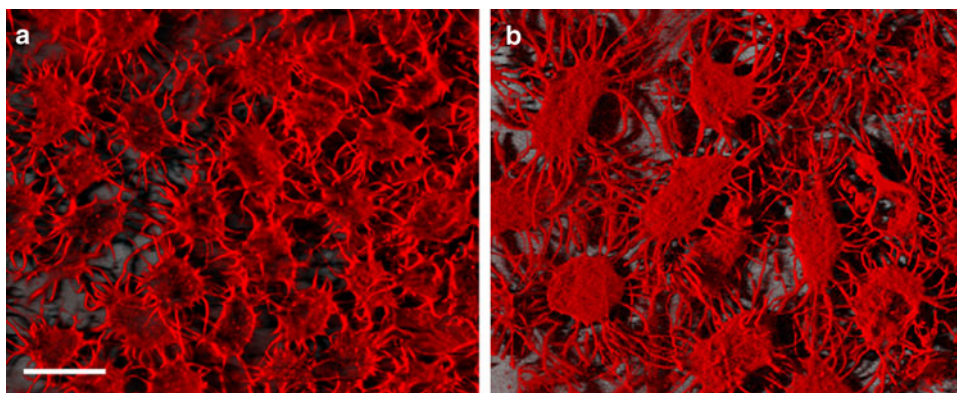


**Table 1** Morphological data of osteocyte network

	Chick parietal bone	Mouse parietal bone
Cell–cell distance ( $\mu\text{m}$ )	$23.5 \pm 6.1$ ( $n = 32$ )	$39.6 \pm 11.6$ ( $n = 32$ )*
Occupancy of bone compartment ( $\mu\text{m}^3$ )	$4,691 \pm 935$ ( $n = 10$ ) <sup>a</sup>	$10,665 \pm 1,510$ ( $n = 12$ )* <sup>a</sup>
Average number of processes radiating from single osteocyte	$52.7 \pm 6.4$ ( $n = 6$ )	$49.7 \pm 9.7$ ( $n = 7$ )
Average length of osteocytes per 1 $\mu\text{m}^3$ of bone compartment ( $\mu\text{m}$ )	$0.24 \pm 0.03$ ( $n = 11$ ) <sup>a</sup>	$0.25 \pm 0.06$ ( $n = 10$ ) <sup>a</sup>
Average surface area of osteocytes per 1 $\mu\text{m}^3$ of bone compartment ( $\mu\text{m}^2$ )	$0.24 \pm 0.08$ ( $n = 10$ ) <sup>a</sup>	$0.25 \pm 0.06$ ( $n = 10$ ) <sup>a</sup>
Average volume of osteocytes per 1 $\mu\text{m}^3$ of bone compartment (%)	$9.71 \pm 1.92$ ( $n = 10$ ) <sup>a</sup>	$12.5 \pm 1.97$ ( $n = 10$ ) <sup>a</sup> *

<sup>a</sup> Number of analyzed regions including several osteocytes

\* Comparison to chick parietal bone  $P < 0.05$

$10,665 \pm 1,510 \mu\text{m}^3$  in the mouse ( $n = 12$ ; Table 1). The bone compartment area of the chick osteocyte was significantly smaller than that of the mouse osteocyte ( $P < 0.05$ ).

#### Morphometric Analysis of Osteocytes in the Unit Bone Matrix

The length of osteocyte processes was obtained using Neuron Tracer software. The length of osteocyte processes per 1  $\mu\text{m}^3$  bone compartment was  $0.24 \pm 0.03 \mu\text{m}$  in the chick and  $0.25 \pm 0.06 \mu\text{m}$  in the mouse ( $n = 11$  and 10, respectively; Table 1).

The surface area and volume were obtained with Surpass software. The average osteocyte surface area per

1  $\mu\text{m}^3$  of the bone compartment was  $0.24 \pm 0.08 \mu\text{m}^2$  in the chick and  $0.25 \pm 0.06 \mu\text{m}^2$  in the mouse ( $n = 10$  and 10, respectively; Table 1). There was no species difference. The volume ratio of osteocytes to bone compartment was  $9.71 \pm 1.92\%$  in the chick and  $12.5 \pm 1.97\%$  in the mouse ( $n = 10$  and 10, respectively; Table 1).

#### Total Length of Processes, Cell Surface, and Volume of One Osteocyte

Each osteocyte had an average volume of  $4,691 \pm 935 \mu\text{m}^3$  in the chick and  $10,665 \pm 1,510 \mu\text{m}^3$  in the mouse. Therefore, the morphometric data per unit bone compartment were multiplied by the mean volume of the

**Table 2** Morphological data of single osteocyte

	Chick parietal bone	Mouse parietal bone
Total length of cell processes ( $\mu\text{m}$ )	$1,131 \pm 139$	$2,668 \pm 596^*$
Cell surface area ( $\mu\text{m}^2$ )	$1,128 \pm 358$	$2,654 \pm 659^*$
Body	666 (59%)	1,067 (40%)
Process	461 (41%)	1,587 (60%)
Cell volume ( $\mu\text{m}^3$ )	$455 \pm 90$	$1,328 \pm 210^*$
Body	332 (73%)	641 (48%)
Process	123 (27%)	688 (52%)

\* Comparison to chick parietal bone  $P < 0.05$

bone compartment occupied by each osteocyte ( $4,692$ ,  $10,665 \mu\text{m}^3$ ) to obtain morphometric data per single osteocyte. As a result, the average values for one chick osteocyte were calculated as follows: cell processes  $1,131 \pm 139 \mu\text{m}$ , surface area  $1,128 \pm 358 \mu\text{m}^2$ , and cell volume  $455 \pm 90 \mu\text{m}^3$  (Table 2). The average values for one mouse osteocyte were calculated as follows: cell processes  $2,668 \pm 596 \mu\text{m}$ , surface area  $2,654 \pm 659 \mu\text{m}^2$ , and cell volume  $1,328 \pm 210 \mu\text{m}^3$  (Table 2). All morphometric data for mouse osteocytes were larger than those for chick osteocytes ( $P < 0.05$ ).

#### FRAP Analysis Showed Dye Coupling Among Osteocytes in Parietal Bone

Living osteocytes in chick and mouse parietal bone were loaded with the fluorescent dye calcein-AM. Figure 4a, d shows a fluorescent image of living osteocytes, which is a single optical slice of chick and mouse parietal bone. Figure 4b, e shows a DIC image at the same location as in Fig. 4a, d. Osteocytes were confirmed to be embedded in lacunae by merging the fluorescent and DIC images (Fig. 4c, f).

FRAP analysis was used to examine functional gap junctions between osteocytes in chick and mouse parietal bone. The rapid recovery of fluorescence into photobleached cells was observed within 5 minutes after photobleaching (Fig. 4g–i). The rapid recovery of fluorescence into photobleached cells was not significantly different between chick and mouse osteocytes within 4 minutes after photobleaching (Fig. 4i). Five minutes after photobleaching, the fluorescence intensity recovered to  $49.0 \pm 2.4\%$  in chick and  $39.9 \pm 2.4\%$  in mouse parietal bone ( $n = 20$  and  $30$ , respectively).

#### Discussion

Our previous studies demonstrated that a 3D analysis of osteocyte morphology by CLS microscopy and FRAP

analysis could be conducted in chick calvariae to investigate the morphology and function of osteocytes in vivo or ex vivo [11, 12]. Although previous studies have compared osteocyte morphology between species, they were performed using 2D morphologic data in different types of bone from various age groups [14–18]. Therefore, in the present study, the 3D morphology of the osteocyte network and cell–cell communication in chick and mouse calvarial parietal bone were analyzed to examine species differences in unified age groups. We observed and analyzed the osteocyte network in the mineralization areas of embryonic calvariae in E16 chicks and E17 mice in the study.

The experimental protocols for the CLS microscopy and FRAP analysis of the mouse calvariae were modified from those used in our previous experiments as the mouse tissue showed much more nonspecific labeling and fewer signals in osteocytes than chick tissue. The nonspecific labeling was derived from the nonspecific uptake of fluorescent materials at the mouse periosteum, which was attached more tightly to the bone surface than in the chick. Hence, more care was taken to detach the periosteum completely from the mouse calvariae. In addition, the mouse samples were  $2 \times 2 \text{ mm}$  in size, whereas the chick samples were  $3 \times 3 \text{ mm}$  in size.

In this study, we confirmed that although the physical characteristics of osteocytes in chick and mouse calvariae are similar, as both have spherical cell bodies with long processes and form intercellular networks, in mice the point-to-point distance between the centers of osteocytes ( $39.6 \mu\text{m}$ ) was significantly greater than that in chicks ( $23.5 \mu\text{m}$ ). In a previous study, Skedros [19] examined the 3D lacuna–lacuna distance (Lc–Lc) in the horse, elk, and sheep but calculated the 3D Lc–Lc lacuna density using 2D segment values in each species; and the range of Lc–Lc distances was only on the order of  $3\text{--}5 \mu\text{m}$  in each species. Furthermore, their results might also reflect age differences as the samples were not taken in the same age groups. Beno et al. reported 3D Lc–Lc distances in the chick, rabbit, bovine, horse, dog, and human [20]. The chick Lc–Lc distance in their report was similar to that in the current study. However, these 3D distances were calculated by combining the 2D osteocyte density of each species and 2D information about osteocyte processes in the mouse; i.e. they did not reflect the real Lc–Lc distance in each species. The current study observed the true 3D osteocyte morphology in bone and determined that the real 3D distance between osteocytes in the mouse was twice as large as that in the chick. There were species differences between chicks and mice with regard to the 3D distances between osteocytes. The shape of the osteocytes was similar between the two species, but their 3D distributions were different.

A single osteocyte occupied  $4,692 \mu\text{m}^3$  of the bone compartment in the chick and  $10,665 \mu\text{m}^3$  in the mouse,

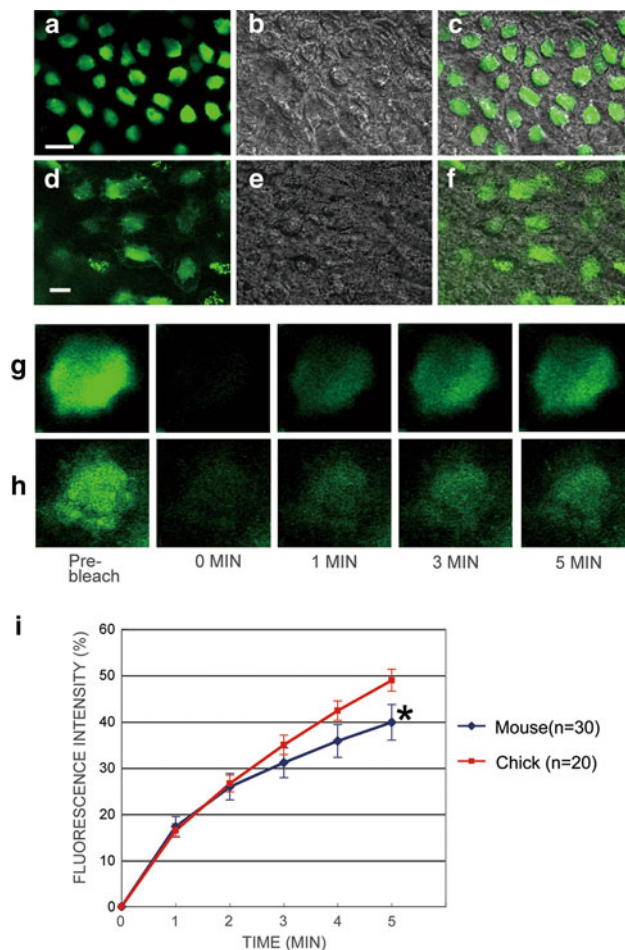


**Fig. 4** Optically sliced images of fluorescently labeled osteocytes by CLS microscopy and FRAP analysis of osteocytes in chick and mouse parietal bone. **a** Fluorescent image of live osteocytes, labeled with calcein, in chick parietal bone. **b** DIC image of lacunae in chick parietal bone. Images were taken at a distance of 9.0  $\mu\text{m}$  from the osteoblast layer. **c** Merged image of **a** and **b**. **d** Fluorescent image of living osteocytes, labeled with calcein, in mouse parietal bone. **e** DIC image of lacunae in mouse parietal bone. Images were taken at 9.0  $\mu\text{m}$  in depth from the osteoblast layer. **f** Merged image of

fluorescent (**d**) and DIC (**e**) images. **g** Images of fluorescently labeled osteocytes in chick parietal bone produced by FRAP analysis. **h** Images of fluorescently labeled osteocytes in mouse parietal bone from FRAP analysis. Serial images were taken prebleach, immediately after bleaching, and at 1, 3, and 5 minutes during fluorescence recovery. **i** Recovery of fluorescence intensity. Data are expressed as the mean  $\pm$  SE. Significant difference at 5 minutes  $*P < 0.05$ . Bar in **a**, **d** = 20  $\mu\text{m}$

and we calculated the osteocyte density in bone from these volumes. Osteocyte density was about 213,000 osteocytes/ $\text{mm}^3$  in chicks and 96,500/ $\text{mm}^3$  in mice, showing that the osteocytes in chick bone were two and a half times more densely packed than those in mouse bone. Both chick and mouse osteocyte density was greater than human osteocyte density, which ranges from 13,900 to 19,400 osteocytes/ $\text{mm}^3$ , as reported previously [22–24]. Our data were not calculated from 2D sections but rather represent the actual 3D density in bone. It has been suggested that the 3D osteocyte distribution in bone differs between species. In relation to this, it is reported that osteocyte density might influence the remodeling rate, mineral apposition rate, mineral homeostasis, and

bone mechanical properties [25–31]. Therefore, these parameters may differ between chicks and mice. However, in order to elucidate the relationship between osteocyte density and these parameters, it would be necessary to analyze long bones and mature bones. We will analyze long bones in the future. Additionally, the total length of cell processes, cell surface area, and cell volume of a single osteocyte in the mouse were two times greater than those in the chick. It is thought that previous osteocyte data from chicks could not be applied to mice without modification. In the present study, we obtained 3D osteocyte morphometric data from mouse bones. These values can be applied to genetically engineered mice in various disease states.

In contrast to the significant difference in osteocyte density between chicks and mice, the average surface area of osteocytes per  $1 \mu\text{m}^3$  in the bone compartment was not significantly different. This suggests that osteocytes in both species have equal ability to respond to external stimuli. In addition, the length of osteocyte processes per  $1 \mu\text{m}^3$  in the bone compartment showed little difference between chicks (0.24  $\mu\text{m}$ ) and mice (0.25  $\mu\text{m}$ ), indicating similar osteocyte process densities. These results suggest that osteocyte processes might play an important role in osteocyte function as, e.g., a mechanosensor. There is a possibility that osteocyte processes in chicks and those in mice sense and respond similarly to the change of external environment.

FRAP analysis of living osteocytes in bone facilitated investigation of GJIC in chick and mouse parietal bone. Our study demonstrated, for the first time, the occurrence of intercellular communication mediated by gap junctions among osteocytes in different species. This study has the advantage that we analyzed this functional intercellular communication in living bone. Therefore, we consider that our data accurately reflect the bone microenvironment in each species. We showed that, in spite of the differences in osteocyte density and size, the recovery of fluorescence in photobleached cells was not significantly different between chick and mouse osteocytes within 4 minutes after photobleaching. These results might be related to osteocyte process density. Five minutes after photobleaching, the fluorescence intensity recovered to 50% of the prebleach level in chick osteocytes and to 40% of the prebleach level in mouse osteocytes. GJIC is thought to have an important role in bone remodeling [12]. A recent study showed that overexpressing connexin43, a major gap junction protein, increased GJIC between bone marrow stromal cells and resulted in an increased volume fraction of bone in vivo [32]. The results of FRAP analysis suggest that the rates of cell–cell communication may affect bone remodeling, bone size, and bone mass in different species. Additionally, the results from FRAP analysis affirm our hypothesis based on morphological data that the chick might exhibit different rates of bone remodeling compared to the mouse.

Some limitations of this study are that these morphological values were only from chick and mouse calvarial parietal bone and the observed specimens were embryonic. However, these fundamental data for osteocytes could be useful. Recent studies have demonstrated various bone phenotypes in some null mutant and/or transgenic mice [33–37]. For such mice, the present analytic methods allow for the further precise investigation of osteocyte morphology, their network, and a part of the functional analysis between osteocytes. The present methods of observation by CLS microscopy are quite straightforward without any need for sample sectioning. As embryonic calvariae are very thin and flat, we were able to stain and visualize them

clearly without decalcification and sectioning. The anatomical features of the calvaria are thus useful for examining live osteocytes in bone. In addition, the organ culture of calvariae, unlike that of long bone, was developed because of their characteristic thin structure and ability to remain competent for long periods of incubation; and this system also allows further experimental manipulations, such as the addition of cytokines, antibodies, siRNA, etc. In the future, we will analyze osteocyte networks in skeletally mature animals.

In summary, this study successfully compared the 3D morphology of the osteocyte network and cell–cell communication in chick calvariae with those in mouse calvariae and yielded interesting results regarding the 3D osteocyte network. The osteocyte body density, 3D distance of osteocytes, and 3D single osteocyte size were significantly different. However, the density of osteocyte processes between chick and mouse embryo calvariae was not different. Also, this study demonstrated for the first time that cell–cell communication occurs via the gap junctions between osteocytes in different species, using FRAP analysis. The recovery of fluorescence intensity in the chicks was higher than that in the mice after 5 minutes. Within 4 minutes, the behavior of recovery was similar between the two species. Osteocyte processes might be related to this behavior because osteocyte processes, which connect to each other via gap junctions in the bone matrix, are thought to play an important role in cell–cell communication. Therefore, it is crucial to observe 3D osteocyte networks including osteocyte processes and live cells in bone in order to understand osteocyte functions. As variations in cell size and cell number cause differences in size and growth between diverse species and as the 3D osteocyte network in bone differed between chicks and mice, it is thought that previous osteocyte data from chicks cannot be applied to mice without modification. Hence, the present study could contribute to a better understanding of the functional roles of the osteocyte network in various species and genetically engineered animals.

**Acknowledgement** This study was supported in part by grants-in-aid for young scientists from the Japan Society for the Promotion of Science.

## References

1. Skerry TM, Bitensky L, Chayen J, Lanyon LE (1989) Early strain related changes in enzyme activity in osteocytes following bone loading in vivo. *J Bone Miner Res* 4:783–788
2. Lanyon LE (1993) Osteocytes, strain detection, bone modeling and remodeling. *Calcif Tissue Int* 53:S102–S107
3. Klein-Nulend J, van der Plas A, Semeins CM, Ajubi NE, Frangos JA, Nijweide PJ (1995) Sensitivity of osteocytes to biomechanical stress in vitro. *FASEB J* 9:441–445



4. Ajubi NE, Klein-Nulend J, Alblas MJ, Burger EH, Nijweide PJ (1999) Signal transduction pathways involved in fluid flow-induced PGE<sub>2</sub> production by cultured osteocytes. *Am J Physiol Endocrinol Metab* 276:E171–E178
5. Bonewald LF, Johnson ML (2008) Osteocytes, mechanosensing and Wnt signaling. *Bone* 42:606–615
6. van der Plas A, Nijweide PJ (1992) Isolation and purification of osteocytes. *J Bone Miner Res* 7:389–396
7. Tanaka-Kamioka K, Kamioka H, Ris H, Lim SS (1998) Osteocyte shape is dependent on actin filaments and osteocyte processes are unique actin-rich projections. *J Bone Miner Res* 13:1555–1568
8. Kamioka H, Ishihara Y, Ris H, Murshid SA, Sugawara Y, Takano-Yamamoto T, Lim SS (2007) Primary cultures of chick osteocytes retain functional gap junctions between osteocytes and between osteocytes and osteoblasts. *Microsc Microanal* 13:108–117
9. Kamioka H, Sugawara Y, Murshid SA, Ishihara Y, Honjo T, Takano-Yamamoto T (2006) Fluid shear stress induces less calcium response in a single primary osteocyte than in a single osteoblast: implication of different focal adhesion formation. *J Bone Miner Res* 21:1012–1021
10. Kamioka H, Honjo T, Takano-Yamamoto T (2001) A three-dimensional distribution of osteocyte processes revealed by the combination of confocal laser scanning microscopy and differential interference contrast microscopy. *Bone* 28:145–149
11. Sugawara Y, Kamioka H, Honjo T, Tezuka K, Takano-Yamamoto T (2005) Three-dimensional reconstruction of chick calvarial osteocytes and their cell processes using confocal microscopy. *Bone* 36:877–883
12. Ishihara Y, Kamioka H, Honjo T, Ueda H, Takano-Yamamoto T, Yamashiro T (2008) Hormonal, pH, and calcium regulation of connexin 43-mediated dye transfer in osteocytes in chick calvaria. *J Bone Miner Res* 23:350–360
13. Feng JQ, Ward LM, Liu S, Lu Y, Xie Y, Yuan B, Yu X, Rauch F, Davis SI, Zhang S, Rios H, Drezner MK, Quarles LD, Bonewald LF, White KE (2006) Loss of DMP1 causes rickets and osteomalacia and identifies a role for osteocytes in mineral metabolism. *Nat Genet* 38:1310–1315
14. Mullender MG, Huiskes R, Versleyen H, Buma P (1996) Osteocyte density and histomorphometric parameters in cancellous bone of the proximal femur in five mammalian species. *J Orthop Res* 14:972–979
15. Remaggi F, Cane V, Palumbo C, Ferretti M (1998) Histomorphometric study on the osteocyte lacuno-canalicular network in animals of different species. I. Woven-fibered and parallel-fibered bones. *Ital J Anat Embryol* 103:145–155
16. Ferretti M, Muglia MA, Remaggi F, Cane V, Palumbo C (1999) Histomorphometric study on the osteocyte lacuno-canalicular network in animals of different species. II. Parallel-fibered and lamellar bones. *Ital J Anat Embryol* 104:121–131
17. Qiu S, Rao DS, Palnitkar S, Parfitt AM (2002) Age and distance from the surface but not menopause reduce osteocyte density in human cancellous bone. *Bone* 31:313–318
18. Vashishth D, Gibson G, Kimura J, Schaffler MB, Fyhrie DP (2002) Determination of bone volume by osteocyte population. *Anat Rec* 267:292–295
19. Skedros JG (2005) Osteocyte lacuna population densities in sheep, elk and horse calcanei. *Cells Tissues Organs* 181:23–37
20. Beno T, Yoon YJ, Cowin SC, Fritton SP (2006) Estimation of bone permeability using accurate microstructural measurements. *J Biomech* 39:2378–2387
21. Wade MH, Trosko JE, Schindler M (1986) A fluorescence photobleaching assay of gap junction-mediated communication between human cells. *Science* 232:525–528
22. Sissons HA, O'Connor P (1977) Quantitative histology of osteocyte lacunae in normal human cortical bone. *Calcif Tissue Res* 22:530–533
23. Qin L, Mak AT, Cheng CW, Hung LK, Chan KM (1999) Histomorphological study on pattern of fluid movement in cortical bone in goats. *Anat Rec* 255:380–387
24. Hazenberg JG, Taylor D, Lee TC (2007) The role of osteocytes and bone microstructure in preventing osteoporotic fractures. *Osteoporos Int* 18:1–8
25. Cownin SC, Moss-Salentijn L, Moss ML (1991) Candidates for the mechanosensory system in bone. *J Biomech Eng* 113:191–197
26. Weinbaum S, Cownin SC, Zeng Y (1994) A model for the excitation of osteocytes by mechanical loading-induced bone fluid shear stresses. *J Biomech* 27:339–360
27. Mullender MG, van der Meer DD, Huiskes R, Lips P (1996) Osteocyte density changes in aging and osteoporosis. *Bone* 18:109–113
28. Skedros JG, Hunt KJ, Dayton MR, Bloebaum RD, Bachus KN (2001) Relative contributions of material characteristics to failure properties of cortical bone in strain-mode-specific loading: implications for fragility in osteoporosis and aging. *Trans Am Soc Biomech* 25:215–216
29. Qui S, Rao DS, Palnitkar S, Parfitt AM (2002) Relationships between osteocyte density and bone formation rate in human cancellous bone. *Bone* 31:709–711
30. Skedros JG, Hunt KJ, Hughes PE, Winet H (2003) Ontogenetic and regional morphologic variations in the turkey ulna diaphysis: implications for functional adaptation of cortical bone. *Anat Rec A Discov Mol Cell Evol Biol* 273:609–629
31. Hernandez CJ, Majeska RJ, Schaffler MB (2004) Osteocyte density in woven bone. *Bone* 35:1095–1099
32. Rosselló RA, Wang Z, Kizana E, Krebsbach PH, Kohn DH (2009) Connexin 43 as a signaling platform for increasing the volume and spatial distribution of regenerated tissue. *Proc Natl Acad Sci USA* 106:13219–13224
33. Yoshida S, Hayashi T, Kunisada M, Ogawa S, Nishikawa H, Okamura T, Sudo LD, Shultz, Nishikawa S (1990) The murine mutation osteopetrosis is in the coding region of the macrophage colony stimulating factor gene. *Nature* 345:442–444
34. Reaume AG, de Sousa PA, Kulkarni S, Langille BL, Zhu D, Davies TC, Juneja SC, Kidder GM, Rossant J (1995) Cardiac malformation in neonatal mice lacking connexin43. *Science* 267:1831–1834
35. Komori T, Yagi H, Nomura S, Yamaguchi A, Sasaki K, Deguchi K, Shimizu Y, Bronson RT, Gao YH, Inada M, Sato M, Okamoto R, Kitamura Y, Yoshiki S, Kishimoto T (1997) Targeted disruption of Cbfa1 results in a complete lack of bone formation owing to maturational arrest of osteoblasts. *Cell* 30:755–774
36. Kong YY, Yoshida H, Sarosi I, Tan HL, Timms E, Capparelli C, Morony S, Oliveira-dos-Santos AJ, Van G, Itie A, Khoo W, Wakeham A, Dunstan CR, Lacey DL, Mak TW, Boyle WJ, Penninger JM (1999) OPGL is a key regulator of osteoclastogenesis, lymphocyte development and lymph-node organogenesis. *Nature* 397:315–323
37. Lecanda F, Warlow PM, Sheikh S, Furlan F, Steinberg TH, Civitelli R (2000) Connexin43 deficiency causes delayed ossification, craniofacial abnormalities, and osteoblast dysfunction. *J Cell Biol* 151:931–943